ACS OMEGA

Open Access

This article is licensed under CC-BY-NC-ND 4.0

http://pubs.acs.org/journal/acsodf

Article

G-Protein-Coupled Receptor 120 Agonist Mitigates Steatotic and Fibrotic Features Triggered in Obese Mice by the Administration of a High-Fat and High-Carbohydrate Diet

Simona Pompili,[†] Alfredo Cappariello,*[,†] Antonella Vetuschi,[‡] and Roberta Sferra[‡]

Cite This: https://doi.org/10.1021/acsomega.4c03507

Read Online

ACCESS | Metrics & More | Article Recommendations

ABSTRACT: Nonalcoholic fatty liver disease (NALFD) represents a complex condition ranging from simple steatosis (nonalcoholic fatty liver, NAFL) to inflammation, and fibrosis is one of the main features of nonalcoholic steatohepatitis (NASH). The pathogenesis of NAFLD is not well established but involves several factors (i.e., predisposition of genetic variants, obesity, and unhealthy lifestyle as unbalanced diets) that lead to an alteration of lipid homeostasis and consequently to an abnormal accumulation of triglycerides and other lipids in the liver parenchyma. Currently, no resolutive pharmacological treatment for NAFLD is available, and the only therapeutic approach is a healthy diet and physical exercise. In this study, we investigated the potential beneficial effect of GprA, a new synthetic agonist of G-protein-coupled receptor 120/free fatty acid receptor 4 (GPR120/FFAR4), in the progression of NAFL/NASH in mice fed for different periods (26 weeks and 30 weeks), with a high-fat (40% kcal) and high-carbohydrate diet, also called a Western-style diet (WSD). In our experimental model, the histological, protein, and transcriptomic analyses highlighted that the GprA can reduce signs of steatosis in WSD-fed mice. Furthermore, in 30 week-treated mice, GprA is also effective in the reduction of collagen deposition and fibrosis development. Altogether, our data validate the central role of FFAR4 in the context of NAFL/NASH onset and progression and reveal that GprA could represent an interesting candidate for the development of a new therapeutic approach in NAFLD treatment.

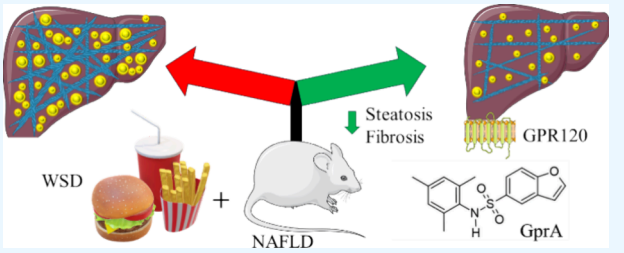

1. INTRODUCTION

Obesity and metabolic abnormalities, such as type 2 diabetes, hypertension, cardiovascular diseases, and steatosis, have recently emerged as one of the most severe health concerns.[1] According to the World Health Organization, in recent years nearly 40% of adults worldwide were overweight and 13% were obese, and metabolic diseases that represent obesity-related conditions continue to increase, affecting the lifestyle of society.[2,3] In recent years, it has been proved that many components of foodstuffs or their metabolites act to control nutrient availability to maintain the body's homeostasis.[4] Nonalcoholic fatty liver disease (NAFLD) is a broad-spectrum hepatopathy ranging from simple steatosis to complex non-alcoholic steatohepatitis (NASH). NAFL is characterized by the presence of hepatic steatosis and rare inflammatory cells without hepatocellular necrosis, while NASH is defined as the association of steatosis, liver inflammation, and hepatocyte ballooning with or without fibrosis which can progress to cirrhosis and hepatocarcinoma (HCC).[5] Although the exact mechanism that drives the development and progression of NASH is unclear, lipotoxic lipid-inflicted cell injury is proposed to be a key contributor.[6] Free fatty acids (FFAs), important nutrients and sources of energy, play a key role in the onset and progression of metabolic abnormalities. FFAs derived from triglycerides and the major long-chain fatty acid present in the plasma (palmitic acid, stearic acid, oleic acid, and linoleic acid) are also signaling molecules that activate several free fatty acid receptors (FFARs) belonging to G-protein-coupled receptors (GPCRs).[7] GPCRs, the largest family of membrane proteins, mediate cellular responses to various stimuli and are able to detect metabolic activity or levels of energy substrates, and most of these receptors play essential roles in the pathophysiology of metabolic disorders, such as diabetes, dyslipidemia, and obesity.[4,8] In particular, G-protein-coupled receptor 120 (GPR120 also known as FFAR4) as well as being involved in the regulation of adipogenesis, inflammation, glucose uptake, and insulin resistance plays a pivotal role in nonalcoholic fatty liver disease (NAFLD) through their function as receptors for bile acid and FFAs.[9] GPR120-deficient mice showed a marked increase in hepatic lipids along with a 10% greater body weight increase than wild-type mice.[10] Abnormal hepatic lipid

Received: April 11, 2024
Revised: June 18, 2024
Accepted: June 20, 2024

Downloaded via UNIV DEGLI STUDI DI L'AQUILA on July 12, 2024 at 10:24:57 (UTC).
See https://pubs.acs.org/sharingguidelines for options on how to legitimately share published articles.

© XXXX The Authors. Published by American Chemical Society

accumulation and the subsequent lipo-toxicity promote NAFLD progression and unhealthy alimentary habits like abuse of a "high-fat diet" are responsible for liver damage.[11−15] A better understanding of NAFL/NASH etiopathology is important for early intervention and identification of potential ways for therapeutic approaches as, to date, treatment of choice for these pathologies has not been established. Lifestyle modification by diet and exercise remains essential to improving the progression of these diseases, but the discovery of a molecule able to decrease lipid accumulation could be crucial for the treatment of these diseases. Healthful dietary patterns and the intake of unsaturated fats are the only available protective strategies against NAFLD, and certain dietary supplements of polyunsaturated FFAs, such as omega-3 fatty acids (ω3-FAs), and probiotics may be helpful, as well. Indeed, in patients with NAFLD, omega-3 supplements at the dose of 4 g/day reduced steatosis, insulin resistance, and inflammation enhancing lipid oxidation and decreasing endogenous lipid production.[16,17] No drugs have been approved to directly treat NAFLD, and the current treatments are only recommended for the management of the associated multisystemic diseases (high blood pressure, diabetes, and hypercholesterolemia).[18−22]

Exploring FFAR signaling to treat metabolic liver disease represents a potential area of research, and more investigation is needed into their hepatic effects. In particular, GPR-120 is an attractive target for developing new pharmacological strategies in NAFLD. Although the perfect animal model able to mimic the complete NAFLD spectrum is not easy to achieve, experimental models based on unbalanced nutritional diets have been shown to elicit an unequivocal NASH stage useful in elucidating intrahepatic events correlated to NASH and test the efficacy of new molecules.[12,13]

To this end, the scientific community has identified several dietary patterns for animals that are useful for inducing the onset of imbalances in liver function that mimic human NAFLD. Among these, we used a model of obesity induced by a high-calorie diet with a high content of sugars and fats, commonly termed the "Western-style diet". This informal name refers to the composition and relative percentage of nutrients, which reflect the eating habits of Western populations, where there is an abuse of foods and beverages rich in fructose and saturated fats, commonly found in the so-called junk food typically consumed in fast food restaurants.

On these bases, we plan to evaluate the potential beneficial effect of a new synthetic agonist of GPR-120 (GprA) in the progression of the diet-induced disease and select the effective concentration of GprA using a mouse model of NAFLD induced by a "Western-style diet (WSD)".

2. MATERIALS AND METHODS

2.1. Chemicals and In Vitro Characterization. N-(2,4,6-Trimethylphenyl)-1-benzofuran-5-sulfonamide (GprA, molecular weight: 315.387; molecular formula: $C_{17}H_{17}NO_3S$; Figure 1A) was synthesized at L'Aquila, Italy. A batch of GprA from the same lot number has been used for the entire treatment to minimize intravariability. The stock solution was made in a buffer vehicle (20% DMSO + 80% 0.1 M pH 8 NaH_2PO_4/NaOH 0.1 N). When necessary, the stock solution was serially diluted in DMSO and then further diluted in assay buffer containing 0.01% BSA.

The receptor compound profiling experiments were done using Chinese hamster ovary (CHO) cells stably transfected by neomycin selection with GPR120 (full length, Origene, CAT#:

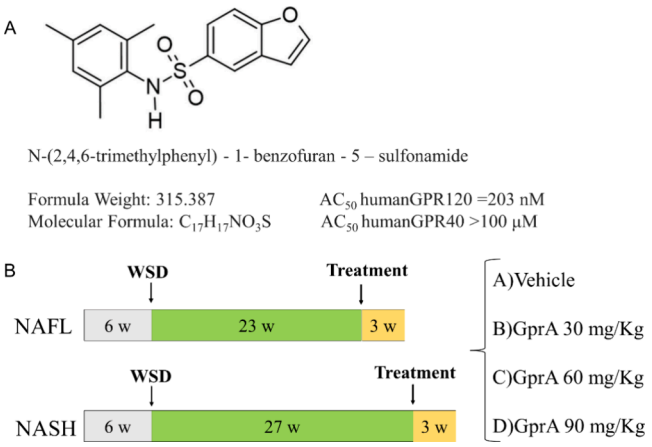

Figure 1. Drug identity and experimental protocol: (A) chemical 2D structure of the compound GprA and properties. (B) Schematization of in vivo experimental procedures, indicating the time frame of phases of the operative protocol: *gray*, weeks of standard growth of animal; *green*: weeks of only administration of WSD; yellow, weeks of treatment with GprA.

RC214159, NCBI reference sequence: NM_181745.4) or GPR40 (CAT#: MR222997, NM_194057). GPR120- and GPR40-CHO were maintained in DMEM/F-12 (1:1) mixture (LONZA), 2 mM ultraglutamine 1 (BioWhittaker cat. BE17−605E/U1), 1 mM sodium pyruvate (LONZA), 7.5% sodium bicarbonate (LONZA), 1 μM Hepes (LONZA), 1× penicillin/streptomycin (LONZA), and 10% fetal bovine serum (Euroclone).

Selectivity on members of other GPCRs was performed at Eurofins Cerep (Celle-Lévescault, France) as a contract service. A summary of the protocol and the reference for the assays are listed on the Eurofins Cerep Website at (https://www.eurofinsdiscoveryservices.com/catalogmanagement/viewItem/SafetyScreen44-Panel-Cerep/P270). The tested receptors are GPL1R, GPR119, GPR43, TGR5, P2 × 3, TRPA1, TPRV1, and TRPV4.

2.2. Metabolic Stability in Microsomes. GprA (1 μM) was dissolved in DMSO and preincubated for 10 min at 37 °C with mouse and human liver microsomes (Xenotech). After the preincubation period, reactions were started by adding the cofactors mixture (NADP, Glc6P, G6P-DH); samples were taken at times: 0, 15, and 30 min by adding acetonitrile to stop the reaction and then centrifuged, and the supernatants were analyzed and quantified by HPLC-MS/MS (Waters Acquity UPLC coupled with a sample organizer and interfaced with a triple quadrupole Waters Premiere XE).

2.3. Calcium-Flux Measurement for Receptor Activation Evaluation By Ligands. GPCR activation has been detected by measuring changes in intracellular Ca^{2+} concentration by using fluorescent imaging based on the emission of calcium-sensitive dye (Fluo8 No Wash Calcium Assay kit, ABD Bioquest, cat. no. 36316). α-Linolenic acid (ALA, Sigma-Aldrich cat. L2376) was used as a reference activator (EC50:5 μM). Transfected GPR120 or GPR40 CHO cells (1×10^4) were seeded in 384 assay plates (Greiner 781091) in complete medium and incubated for 24 h (incubator at 37 °C/5% CO2/90% humidity). Thus, Fluo8 dye was incubated for 2 h, and finally, GprA was tested in a dose-dependent manner (8 concentrations starting from 100 μM in triplicate and with a 0.5 log distance between concentrations) by adding to cells, washed (5 times), and the emitted fluorescence was monitored over 7

https://doi.org/10.1021/acsomega.4c03507
ACS Omega XXXX, XXX, XXX−XXX

min. Thereafter, reference agonist at ∼EC50 (5 μM ALA) was added to the cells, and the emitted fluorescence was monitored over 3 min. Finally, 2.8 mM Ca^{2+} was added, and emitted luminescence was then recorded. Background control was performed incubating cells only with the vehicle of Fluo8, namely, Tyrode's buffer (130 mM NaCl, 5 mM KCl, 2 mM CaCl2, 1 mM MgCl2, 5 mM $NaHCO_3$, 20 mM HEPES, pH 7.4, sterile filtered).

2.4. Experimental In Vivo Procedures. Procedures involving animals and their care were conducted in conformity with national and international laws and policies (European Economic Community Council Directive 86/609, OJ L 358, 1, December 12, 1987; Italian Legislative Decree 4.03.2014 n.26, Gazzetta Ufficiale della Repubblica Italiana no. 61, March 4, 2014; National Institutes of Health Guide for the Care and Use of Laboratory Animals, National Institutes of Health Publication no. 85−23, 1985) and were approved by the Ministry of Health at the University of L'Aquila (618/2021-PR Risp a prot CE5C5.37).

2.4.1. Pharmacokinetics and Liver Uptake of GprA. Pharmacokinetics of GprA was investigated after a single oral administration in a group of six male C57/BL/6N mice subjected to treatment with GprA (90 mg/kg). Evaluation was carried out on blood, and liver samples were collected from three animals per group sacrificed after 1 h and three mice after 4h from administration. Briefly, the hind leg was shaved until the saphenous vein was visible and punctured using a 20 G needle, and ∼30 μL of blood was collected in prelabeled prechilled tubes. After the collection of blood samples at each time point, the blood samples were stored on ice prior to centrifugation at 2500*g* for 15 min at 4 °C within 0.5 h of collection to separate plasma. Immediately after blood withdrawal for PK estimation, whole blood was collected, the chest of the mice was exposed, and animals were subjected to whole-body perfusion. After perfusion, the liver was separated. Explanted tissues were immediately weighed and stored at −80 ± 10 °C until homogenization. After isolation, tissues were suspended in PBS 0.1 M pH 8 (NaH2PO4/NaOH 0.1N)/methanol/Tween 20 (5.8:4:0.2 v/v/v) in the 1 g: 5 mL ratio and homogenized on ice with an Ultra-Turrax (Ika-Werk) homogenizer three times for 30 s. The tissues after homogenization were sonicated on ice three times for 30 s. Samples were ultracentrifuged (Sorvall centrifuge) for 20 min at 5000 rpm at 4 °C. The supernatant was withdrawn and diluted with methanol in a 1:3 v/v ratio and ultracentrifuged for 10 min at 14,000 rpm at 4 °C. The resulting supernatant was used for HPLC-MS analysis.

2.4.2. Animal Model of Nonalcoholic Fatty Liver Disease and Drug Treatment. A total of sixty-four C57/BL/6N male mice were purchased from *Taconic Biosciences* (*Lille Skensved*-4623, DK) specialized in a mouse model of nonalcoholic fatty liver disease (NAFLD) induced by hyperglucidic and hyperlipidic diet (Western-style diet, WSD). The NAFL group consisting of 32 male mice arrived after 20 weeks of WSD diet (D09100310i, Research Diet, Table 1), while NASH (32 male mice) arrived after 24 weeks of the WSD diet. This diet is known to induce signs resembling histological and metabolic alterations and was extensively used and described in the literature. Upon their arrival at our facility (L'Aquila, Italy), mice were fed with the same diet for a further 3 weeks under the following conditions: temperature: 20−24 °C; humidity: 60% ± 5%; dark/light cycle: 12/12 h to ensure the acclimation. The animals had access to food and water *ad libitum*. For these studies, mice were littermates and were randomized into four subgroups for each group via an online tool (True Random Number Generator, https://www.random.org/). Mice were thus subjected to treatment with the different concentrations of the agonist molecule of GPR-120 (GprA, 30 mg/kg; 60 mg/kg; 90 mg/kg) administered daily, by oral gavage, for 3 weeks (Figure 1B). Control groups received daily vehicle transport by oral gavage. Animal weight was monitored every week. No adverse events were observed during the experiment, except for one vehicle-treated and four GprA-treated mice (randomly for both dose and disease stage).

Table 1. Composition of Diet Used in This Study[a]

	D09100310i		D09100304i	
product	g %	kcal %	g %	kcal %
protein	22	20	19	20
carbohydrate	**45**	**40**	67	70
fat	**20**	**40**	4	10
total		100		100
kcal/g	**4.5**		3.8	
ingredient	g	kcal	g	kcal
casein	200	800	200	800
L-cystine	3	12	3	12
corn starch	0	0	350	1400
maltodextrin 10	100	400	85	340
fructose	**200**	**800**	0	0
dextrose	0	0	169	676
sucrose	96	384	96	384
cellulose	50	0	50	0
soybean oil	25	225	25	225
palm oil	**135**	**1215**	0	0
lard	20	180	20	180
mineral mix S10026	10	0	10	0
dicalcium phosphate	13	0	13	0
calcium carbonate	5.5	0	5.5	0
potassium citrate, 1 H_2O	16.5	0	16.5	0
vitamin mix V10001	10	40	10	40
choline bitartrate	2	0	2	0
cholesterol	**18**	0	0	0
FD&C yellow dye #5	0	0	0.025	0
FD&C blue dye #1	0.025	0	0	0
FD&C red dye #40	0.025	0	0.025	0

[a]The commercially available hypercaloric and hyperlipidic diet cat# D09100310i has been administered to mice according to the scheme reported in Figure 1. The composition of the diet cat# D09100304i is reported only for reference purposes for comparison with the control standard diet routinely used for the maintenance of mice.

At the end of the experimental procedures, the animals were euthanized by carbon dioxide (CO_2) inhalation according to the approved guidelines and under the supervision of a veterinarian. The livers were explanted, weighed, photographed, and dissected. A fragment of the organ was perfused with 4% formalin buffered for 3 h at room temperature for histological, immunohistochemical, and immunofluorescence analyses. The remaining tissue specimens were stored at −80 °C for Western blot and real-time PCR analysis.

2.5. Histopathologic Analysis. Livers were fixed in 4% formalin buffered in phosphate buffer saline (PBS) at pH 7.4 for 3h at room temperature followed by the standard procedure for paraffin embedding. Serial 3 μm sections were stained with hematoxylin and eosin (H&E) to assess the degree of steatosis, ballooning, and inflammation and with Sirius red to detect connective tissue deposition and fibrosis. The stained sections

https://doi.org/10.1021/acsomega.4c03507
ACS Omega XXXX, XXX, XXX−XXX

were then observed under an Olympus BX51 light microscope (Olympus Optical Co. Ltd., Tokyo, Japan; objective lenses Olympus UPlanFI 10x/0.30 Japan, and UPlanFl 20x/0.50 ∞/0.17). Images were captured using Camera Tucsen USB 2.0 H Series and processed using Tucsen TCapture.ink imaging software. Two independent pathologists examined and scored all histological sections of the liver samples in a double-blind based on the parameters described by Kleiner et al. and Bedossa et al.[23,24] Steatosis was graded as 0 (<5%), 1 (5−33%), 2 (33−66%), or 3 (>66%). For each specimen, four fields were evaluated (10× magnification). Ballooning was scored as 0 (none), 1 (few ballooned cells), and 2 (many ballooned cells or prominent ballooning of cells).

Inflammation was defined as a focus of two or more inflammatory cells within the lobule. All foci were counted at 20× magnification (0: none; 1: ≤2 foci; 2: >2 foci). Stage of fibrosis was assigned a score of 0 (none), 1 (perisinusoidal zone or periportal fibrosis), 2 (perisinusoidal and periportal fibrosis without bridging), 3 (bridging fibrosis), or 4 (cirrhosis).

2.6. Oil Red O Staining. Livers were snapped in liquid nitrogen, embedded in the OCT compound, and stored at −80 °C. Serial 8 μm sections were air-dried for 20 min, washed in PBS, and fixed in 10% formalin for 5 min. The slides were washed with 60% isopropyl alcohol, stained with oil red O solution (O1391, Sigma-Aldrich, Merck KGaA, Darmstadt, Germany) for 15 min, and then counterstained with hematoxylin. The stained sections were then observed under an Olympus BX51 light microscope (Olympus Optical Co. Ltd., Tokyo, Japan).

2.7. Hepatic Triglyceride (TG) Analysis. Analysis of hepatic TG was performed on 30 mg of the liver using the Triglyceride Quantification Colorimetric/Fluorometric kit (MAK266, Sigma-Aldrich, Merck KGaA, Darmstadt, Germany) according to the manufacturer's instructions.

2.8. RNA Extraction, Reverse Transcription, and Real-Time Quantitative PCR. Total RNA from the fragments of livers kept at −80 °C was extracted using the RNeasy Plus Mini Kit (Qiagen, cat. No. 74134) according to the manufacturer's instruction. Then RNA (0.8 μg) was reverse-transcribed via RT. cDNA was subjected to real-time PCR using the PowerUp SYBR Green Master Mix (Thermofisher, cat. no. A25741), together with gene-specific primers (Thermo Fisher, Table 2). Reactions were set up in Primo FrameStar 96-well PCR plates (Euroclone, cat. ECPCR0770C), which were sealed with MicroAmp optical adhesive films (Applied Biosystems, cat. 4360954). The thermal profile of the Cielo 6 qPCR system (Azure Biosystem, Dublin, CA, USA) was set as follows: 2 min at 95 °C, then 45 cycles with 15 s at 95 °C and 20 s at 60 °C, along with a final postread stage of 30 s at 60 °C. Data have been analyzed by Azure Cielo Manager software (Azure Biosystem).

Table 2. List of Primers

gene	sequence (5′ → 3′)
mactb FW	CCACCATGTACCCAGGCATT
mactb RW	CGGACTCATCGTACTCCTGC
mccn2 FW	AGCAGCTGGGAGAACTGTGT
mccn2 RW	GCTGCTTTGGAAGGACTCAC
mffar1 FW	AAACTGCGACTCACTCCCAG
mffar1 RW	CGTAGAGGGGAGCAAAGTGG
mffar4 FW	CCGTTCTGGGGCTCATCTTT
mffar4 RW	ACGACGAGCACTAGAGGGAT
mil1b FW	TGCTGCTCAATTATGCCAAG
mil1b RW	TGCTTCTAGCTGGGCAATCT
mil6 FW	AGTTGCCTTCTTGGGACTGA
mil6 RW	TCCACGATTTCCCAGAGAAC
mplin2 FW	GGGGATGGTGCAGTTCATGA
mplin2 RW	TTGCTCGGCTTCTGAACCAT

2.9. Western Blot Analysis. Liver fragments were lysed in RadioImmunoPrecipitation Assay (RIPA) buffer (50 mM Tris−HCl, pH 8.0, with 150 mM sodium chloride, 1.0% NP-40, 0.5% sodium deoxycholate, and 0.1% sodium dodecyl sulfate, Sigma-Aldrich) and proteinase inhibitor cocktail (#P2714, Sigma-Aldrich). Protein content was quantified by the bicinchoninic acid assay (no. 23225, Thermo Fisher Scientific). Twenty-five micrograms of proteins were separated by SDS-PAGE in reducing conditions and blotted onto the nitrocellulose membrane, which was incubated overnight at 4 °C with primary anti-CTGF (1:250, cat. sc-365970, Santa Cruz Biotechnology) antibody. After 1 h of incubation at room temperature with horseradish peroxidase (HRP)-mouse IgG (1:2000, cat. sc-525409, Santa Cruz Biotechnology), bands were visualized by the Super Signal West Pico chemiluminescent substrate (no. RA227125, Thermo Fisher Scientific) and acquired on Chemidoc (Biorad). The loading control was evaluated by extensively washing membranes in T-TBS (5 times for 10 min) and incubating for 1 h at room temperature with primary Actin B (1:200; cat. ab8229, Abcam, Cambridge, UK) followed by a 1 h incubation at room temperature with horseradish peroxidase (HRP)-goat IgG (1:2000, cat. sc-2006, Santa Cruz Biotechnology).

2.10. Immunohistochemistry and Immunofluorescence Analyses. For immunohistochemical analyses, serial 3 μm sections of liver fragments were incubated for 40 min in methanol and then in a 3% hydrogen peroxide solution for 5 min. The specimens were incubated overnight at 4 °C with specific antibodies: COL1A1 and COL3A1 (cat. sc-293182 and sc-8781, respectively; Santa Cruz Biotechnology Inc.) at 1:50 dilutions. The samples were washed in PBS for 5 min and incubated with a streptavidin−biotin-peroxidase-conjugated secondary antibody (K0675, Dakocytomation, Milano, Italy). Once rinsed in PBS for 10 min, the sections were incubated with 3,30-diaminobenzidine tetrahydrochloride for 1 to 3 min. Finally, the specimens were counterstained with Mayer's hematoxylin, mounted, and observed under the Olympus BX51 light microscope (Olympus, Optical Co. Ltd.).

For immunofluorescence (IF) staining, nonspecific protein binding was blocked with 10% bovine serum albumin (BSA) in PBS for 2 h at room temperature. Sections were incubated overnight at 4 °C with anti-smooth muscle alpha-actin (α-SMA, cat. orb310036, Biorbyt Ltd., Cambridge, CB4 0WY, UK) used at dilutions of 1:50. After rinsing in PBS for 10 min three times, sections were incubated with m-IgGκ BP-CFL 594 (cat. sc-516178, Santa Cruz Biotechnology Inc., Santa Cruz, CA, USA). The secondary antibody was diluted 1:200 and incubated at room temperature for 1 h. Sections were treated with mounting medium from Vector Laboratories containing DAPI and photographed with an Olympus BX51 microscope (Olympus, Optical Co. Ltd.). Semiquantitative evaluation of immunohistochemical staining was performed using the immunohistochemistry profiler, a plugin of the digital image analysis public domain software ImageJ version 1.52a (U.S. National Institutes of Health, Bethesda, MD, USA). Four random microscopic fields from all experimental groups were photographed at the same magnification and analyzed. Data were expressed as a

https://doi.org/10.1021/acsomega.4c03507
ACS Omega XXXX, XXX, XXX−XXX

Table 3. In VitroEvaluation of GprA[a]

physicochemical properties								
pK_a			logP			logD		
10.02 ± 0.07			3.57 ± 0.05			3.57		
selectivity toward GPCRs								
receptor	GLP1R	GPR119	GPR43	TGR5	P2 × 3	TRPV1	TRPV4	TRPA1
AC50 (μM)	>100	>100	>100	>100	30	30	30	36.2
stability								
assay						half life (min)		
liver microsomes (mouse)						33 min		
liver microsomes (human)						48 min		

[a]Analysis of physiochemical properties, receptor selectivity, and stability of GprA. Acidic dissociation constant, pK_a; partition coefficient, *P*; distribution coefficient, *D*.

percentage of the positive area and presented as the mean ± standard deviation.

2.11. Statistical Analysis. Data were reported as the mean of ± SEM. The Student's *t* test or ANOVA (with posthoc Mann−Whitney's *U* test for multiple comparisons) was used to determine differences between groups for normally or not normally distributed data, respectively, at $p \leq 0.05$ (GraphPad Prism 7.00; GraphPad Software, Inc., La Jolla, CA, USA).

3. RESULTS

3.1. In Vitro Characterization of GprA. Physiochemical properties (acidic dissociation constant, pK_a, lipophilicity: partition coefficient, *P*, in octan-1-ol/water, and distribution coefficient, *D*) of GprA were determined (Table 3). To examine the ability of our compound GprA to effectively activate GPR120 with high selectivity over the cognate receptor GPR40, we developed a functional cell-based assay. Since both receptors have been shown to couple to Gαq/11-initiated signal transduction pathways and, as such, to induce Ca2+ intracellular spikes, we first evaluated the efficacy of GprA in a Ca2+ mobilization assay using Chinese hamster ovary (CHO) cells stably transfected with the human *ffar4* or *ffar1* gene. GprA showed an AC_{50} = 203 nM on human GPR120 full isoform, thus demonstrating its capacity to bind and activate the receptor (Figure 1). A similar experiment was conducted on CHO cells stably transfected with human GPR40, showing that the GprA induces activation of GPR40 at 500 times higher (>100 μM) than that used before. Thus, we can conclude that GprA is a selective agonist of GRP120. A larger characterization of the receptor selectivity toward other G-protein-coupled receptors (GPCRs) has been carried out, confirming the specificity for GPR120. Finally, the metabolic stability of GprA was assessed in mouse and human microsomes.

3.2. GprA Impact on Macroscopic Parameters of Mice under WSD. To evaluate the effect of GprA on the body weight of mice fed with WSD, the weight of the animals was monitored every week. The fold changes in body weights during the treatments were reported in the graph (Figure 2A).

The GprA administration until 26 weeks is efficacious in reducing body weight at every dosage compared to the vehicle, but differences have not been found among the doses (Figure 2A). Interestingly, at 30 weeks, the dosage of GprA at 30 mg/kg is not efficacious compared to that of the vehicle, while a dose-dependent reduction of body weight is evidenced between 60 and 90 mg/kg compared to the vehicle at 30 weeks (Figure 2A). Macroscopic evaluation of liver weight and the ratio of liver weight/body weight was also conducted to assess the effect of

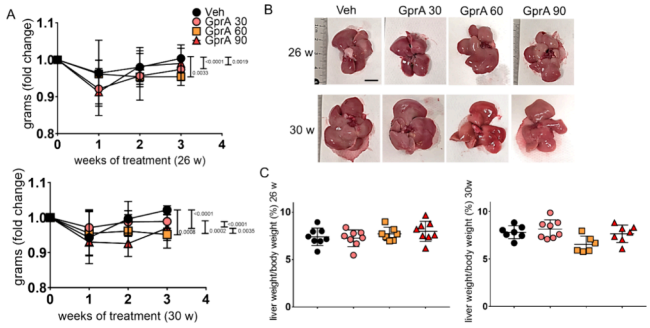

Figure 2. (A) Evaluation of body weight during the treatments. GprA is able to reduce body weight in both NAFL (26 weeks) and NASH (30 weeks) mice. A dose-dependent effect at 30 weeks of diet was found. Statistics: ANOVA among AUC, $p < 0.05$. (B) Gross evaluation of the liver morphology. The photographs highlighted no macroscopic differences among the groups. (C) Liver weight and body weight ratio. The graphs report the liver weight and the liver weight normalized to body weight. Statistics (ANOVA) showed no significant differences among the groups.

GprA in mice under WSD (Figure 2B,C). No significant differences in these parameters were found among the groups, after both 26 and 30 weeks of the WSD diet (Figure 2C).

3.3. Effect of GprA on NAFLD Features of Liver Parenchyma Induced by WSD. The key features of NAFLD (steatosis, ballooning, and inflammation) were first assessed by Hematoxylin and Eosin staining. We noted that only GprA 90 mg/kg (GprA 90) was able to reduce steatosis, especially macrovesicular steatosis, both at 26 and 30 weeks induced by WSD administration (Figure 3A), as reported by the graph of steatosis score (Figure 3B).

The presence of clusters of ballooning hepatocytes, with round shapes and pale cytoplasm, usually reticulated, was found in all groups (Figure 3A, head-arrow), as quantified in the graph (Figure 3C).

Analyses for the biodistribution of GprA revealed that only the 90 mg/kg dosage reached liver parenchyma at a concentration suitable for exerting a biological effect, partially explaining the previous results (Table 4).

On this basis, we further investigated only the effect of 90 mg/kg dosage (GprA90) compared to the vehicle. First, we looked at the expression of receptors *ffar4* and *ffar1*, and no differences were found after 30w of treatment, excluding that GprA can induce modulation of the main target receptor and any compensatory effect on the cognate receptor (Figure 4A).

https://doi.org/10.1021/acsomega.4c03507
ACS Omega XXXX, XXX, XXX−XXX

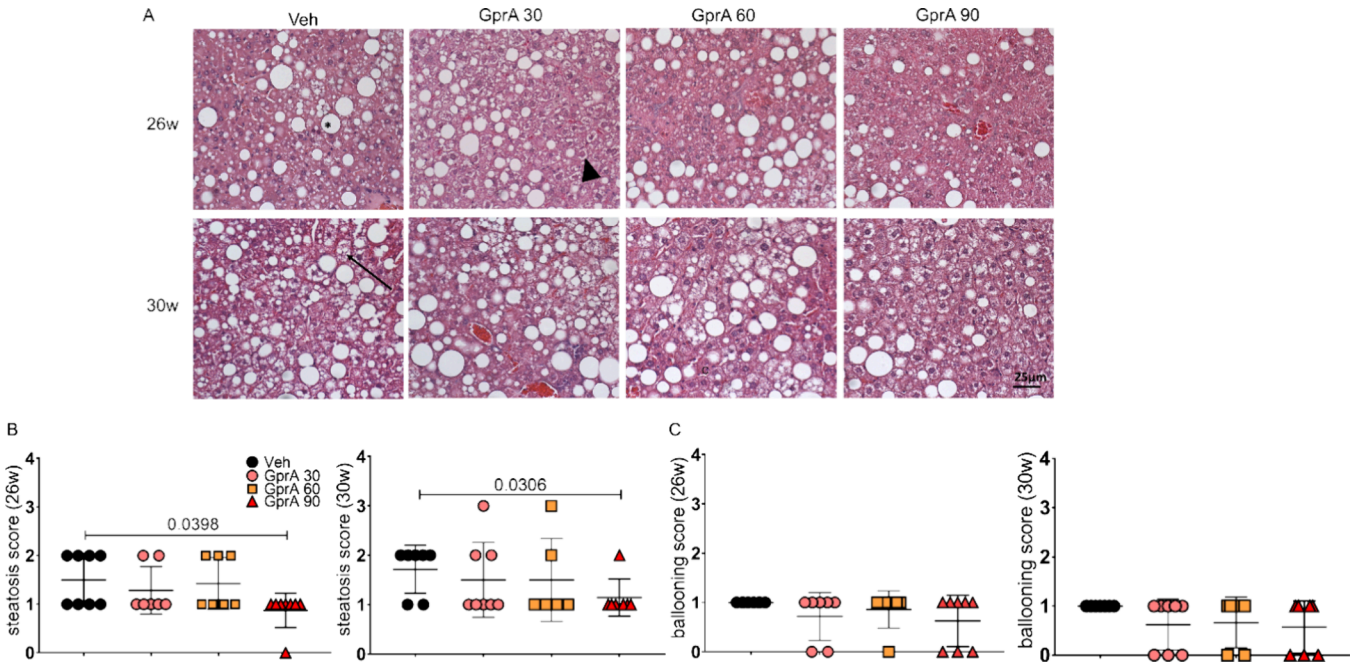

Figure 3. (A) Evaluation of liver phenotype by hematoxylin and eosin. The figures showed a reduction of macrovesicular steatosis (asterisk) and microvesicular steatosis (arrow). Indeed, no differences emerged in the ballooning degeneration (head-arrow) among the groups. (B) Evaluation of steatosis score. At both 26 and 30 weeks, GprA is able to reduce the droplet number compared to vehicle only at the dosage of 90 mg/kg as reported in the graphs. Statistics: Student's *t* test, Veh vs GprA 90 ($p < 0.05$). (C) Evaluation of ballooning degeneration. The ballooning degeneration as scored in the graphs without any significant differences among the groups. Statistics: ANOVA, $p < 0.05$.

Table 4. Evaluation of the Biodistribution of GprA[a]

plasma concentration (ng/mL) of GprA after oral *gavage* (90.0 mg/kg)					
time (h)	M1	M2	M3	mean	std dev
1	68.01	92.84	28.32	63.06	32.54
4	19.54	8.703	19.50	15.92	6.24
liver concentration (ng/g) of GprA after oral *gavage* (90.0 mg/kg)					
time (h)	M1	M2	M3	mean	std dev
1	2535.18	627.59	2247.5	1803.44	1028.42
4	333.72	160.98	1394.8	629.83	668.08
liver/plasma ratio of GprA after oral *gavage* (90.0 mg/kg)					
time (h)	M1	M2	M3	mean	std dev
1	37.28	6.76	79.35	41.13	36.45
4	17.07	18.50	71.52	35.70	31.03

[a]Quantification of GprA (ng) in blood and liver was performed on a total of $n = 6$ male mice ($n = 3$ mice/time point).

Regarding the steatosis, biochemical evaluation for liver triglycerides did not reveal a net difference at 26 weeks for the fat content between vehicle- and GprA-treated mice, while it confirmed a reduction of tissue triglycerides at 30 weeks in the GprA90 group compared to that in the control one (Figure 4B). This evaluation was further deepened by Oil Red staining on liver sections at 26 and 30 weeks, revealing the ability of GprA90 at 26 weeks to decrease not the total number but the area of the lipid droplets (Figure 4C,D), indicating that the same amount of fats are differentially distributed in the parenchyma of liver under GprA treatment, while the effect of GprA becomes apparent at 30 weeks, conciliating this result with the previous pathologist evaluation of the steatosis score (Figure 3A,B). Moreover, looking at gene expression of *plin2* at 26 weeks, we found a slight but significant reduction in GprA90-treated mice at 26 weeks compared to that in vehicle-treated NASH mice, corroborating that GprA already started to exert effects at 26 weeks, although becoming evident later at 30 weeks (Figure 4E).

Furthermore, we assessed the inflammation pattern at 30 weeks, when it is supposed to be more apparent. The gene expression for inflammatory genes *il1b* and *il6* showed nonsignificant modulation between the control and GprA90 groups (Figure 5 A). Coherently, no significant differences in lobular and/or pericellular inflammation were found between Veh and GprA90 at 30 weeks of WSD. Indeed, sporadic inflammatory foci were present in all groups (Figure 5B), as confirmed by the inflammation score (Figure 5B).

3.4. Effect of GprA 90 mg/kg on Liver Fibrosis in NASH Mice. Fibrosis was first evaluated by Sirius red staining (Figure 6A). Veh-treated mice at 30 weeks showed periportal and perisinusoidal fibrotic septa, occasionally with bridging fibrosis. GprA90 was efficacious in reducing fibrotic degeneration as shown both by fibrotic area and by fibrosis score evaluation (Figure 6A).

Next, collagens type I and III were also evaluated by immunohistochemistry (Figure 6B). A considerable net of both collagen I and III positive fibers was highlighted in the liver parenchyma of Veh-treated mice, while GprA90-treated mice showed collagen expression mainly in the wall vessels (Figure 6B), coherent with Sirius red staining. To deeply evaluate the fibrotic profile, we looked at the activation of hepatic stellate cells by immunofluorescence staining for alpha-smooth muscle actin (alpha-SMA) performed at 30 weeks (Figure 7A). A significant decrease in alpha-SMA-positive cells was observed in the GprA90-treated group compared to Veh 30 weeks (Figure 7B). The data confirmed the ability of the GprA to reduce the activation of a myofibroblast-like cell and consequently of the fibrogenesis process.

Finally, we tested the expression of Connective Tissue Growth Factor (CTGF, a downstream effector of TGFβ) and

https://doi.org/10.1021/acsomega.4c03507
ACS Omega XXXX, XXX, XXX−XXX

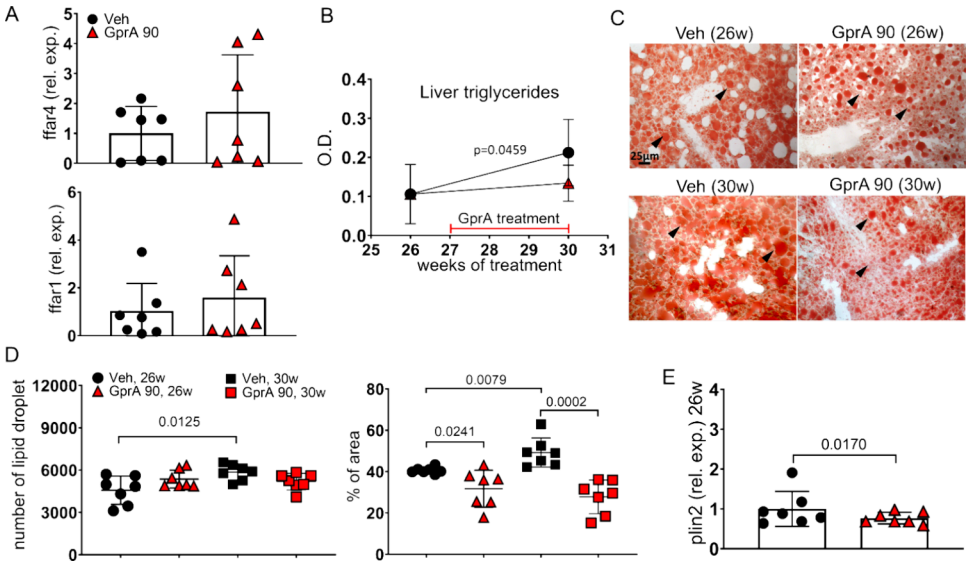

Figure 4. Evaluation of steatotic profile in the liver. (A) Evaluation of gene expression in the liver. RT-PCR on mRNA extracted from livers of animals fed with WSD for 30 weeks (NASH) treated with vehicle (Veh) or GprA 90 mg/kg (GprA 90) for evaluating the expression of *ffar4*, *ffar1*. (B) Biochemical evaluation of triglycerides. Liver triglycerides were extracted from liver homogenates and titrated by spectrometric analysis. Optical density (O.D.) values were normalized for tissue fragment weight (around 30 mg for sample). Statistics, ANOVA ($p < 0.05$) on AUC between Vehicle and GprA. (C) Histological analysis for fat infiltration. Oil red staining showed fat deposition in liver parenchyma (head arrows) at 26 and 30 weeks. (D) Quantification of oil red staining. The number and area of lipid droplets were assessed by oil red staining and normalized for section area. Statistics, ANOVA, $p < 0.05$). (E) RT-PCR on mRNA extracted from livers of animals fed with WSD for 26 weeks (NASH) treated with vehicle (Veh) or GprA 90 mg/kg (GprA 90) for evaluating the expression of *per2*. Results are the mean + SD (n = 7/group). Statistics, Student's t test, $p < 0.05$.

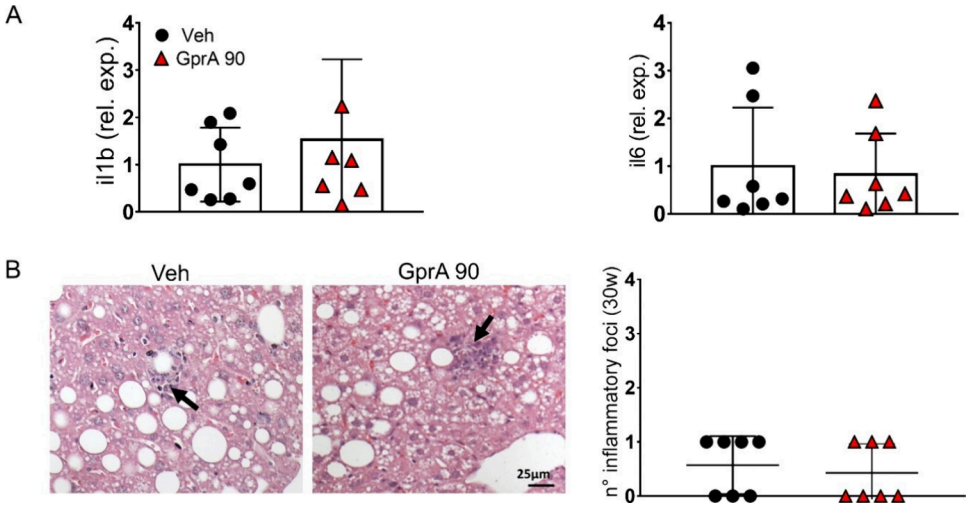

Figure 5. (A) Evaluation of inflammation genes in the liver at 30 weeks. RT-PCR on mRNA extracted from livers of animals fed with WSD for 30 weeks (30 weeks, NASH) treated with vehicle (Veh) or GprA 90 mg/kg (GPRA90) for evaluating the expression of il1b and il6. (B) Evaluation of inflammation index in the liver parenchyma. Foci of inflammatory cells were found in all experimental groups (arrow), without any differences among the groups, as highlighted by the graphs of inflammation score. Results are the mean + SD (n = at least 6/group). Statistics, Student's t test, $p < 0.05$.

found a reduction at transcript (*ccn2*, Figure 7C) and protein (Figure D) levels, confirming the decrease of the pro-fibrotic marker.

4. DISCUSSION

NAFLD is a complex group of metabolic multifactorial disorders with a high incidence in the adult population, including NAFL and NASH. The main risk factor is obesity, often caused by an unhealthy lifestyle characterized by high caloric intake, the abuse of unsaturated fats, and limited physical activity. Under physiological conditions, fats are stored in the adipose tissue, but the overcoming of its storing capability due to an unbalanced diet leads to insulin resistance (IR) of the adipose tissue, which causes a low grade of systemic inflammation and ectopic fat accumulation, mainly in the liver.[25,26]

Indeed, the liver is primarily involved in the metabolism of lipids and glucose. About 60% of fat processed in the liver is derived from the dysfunction of adipose tissue, while the other 40% of fat comes from dietary carbohydrates and is converted to free fatty acids (FFAs) by de novo lipogenesis.[27,28] High caloric intake leads first to a toxic effect on the liver and finally to NAFLD.[29] FFA accumulation, due to the increase of lipogenesis, dysfunction in mitochondrial beta-oxidation, and reduction of very low-density lipoproteins (VLDL) secretion, leads to liver

https://doi.org/10.1021/acsomega.4c03507
ACS Omega XXXX, XXX, XXX−XXX

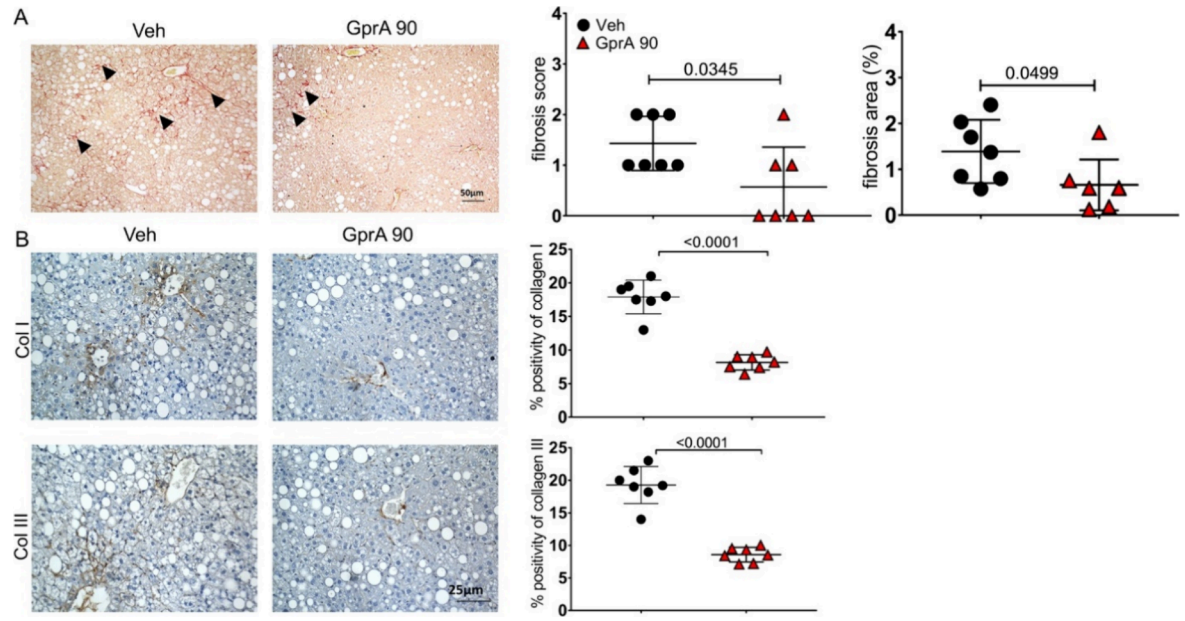

Figure 6. Evaluation of fibrosis. (A) Sirius red staining in the liver parenchyma. Left: microphotograph for collagen deposition evidenced by Sirius Red staining (head arrows) in the livers of Veh- and GprA90-treated mice. Right: the fibrosis score and fibrosis area were calculated and reported in the graphs. Results are the mean + SD (n = 7/group). Statistics, Student's t test, $p < 0.05$. (B) Immunohistochemistry for collagens I and III and relative quantifications. Microphotographs for collagens I and III positivity in the livers of mice after 30 weeks of WSD upon Veh or GprA90 administration. Statistics, Student's t test, $p < 0.05$.

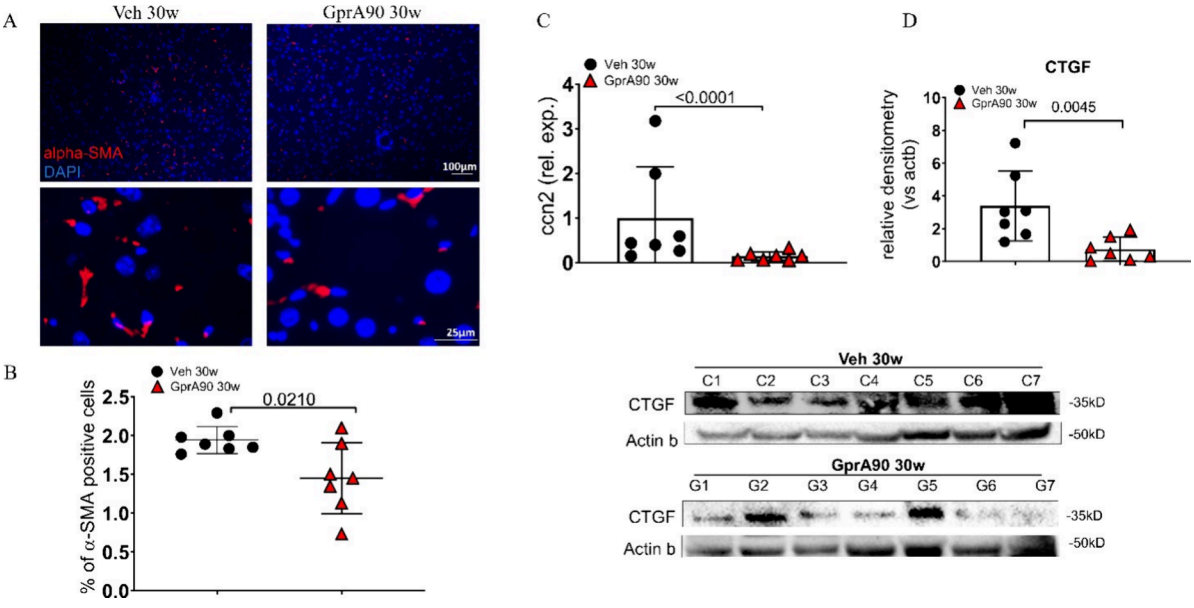

Figure 7. Evaluation of the fibrotic network. (A) Immunofluorescence (upper line, low magnification; bottom line, high magnification) for alpha-smooth muscle actin (α-SMA, red: Alexa fluor-594 conjugated; blue: nuclear counterstaining by diamidino-2-phenylindole, DAPI) and (B) relative quantification in livers of animals fed with WSD for 30 weeks (NASH) treated with vehicle (Veh) or GprA 90 mg/kg (GprA90). (C) RT-PCR on mRNA extracted from livers for evaluating the expression of the ccn2 gene. (D) Quantification of WB analysis (bottom) on protein lysates from NASH vehicle-treated control (C1−C7) livers and GprA-treated (G1−G7) livers for evaluating the expression of CTGF (actin beta has been used as a loading control). Results are the mean ± SD (n = 7/group). Results are the mean ± SD (n = 7/group). Statistics: Student's t test, $p < 0.05$.

steatosis. Then, the Kupffer cells become engulfed with large amounts of FFAs, driving them toward an inflammatory phenotype and the release of inflammatory cytokines. These events cause low-grade inflammation in liver parenchyma and participate in activating the trans-differentiation of hepatic stellate cells (HSCs) into collagen-producing myofibroblasts, finally triggering fibrosis and NASH progression.[30−32] Finally, multisystemic syndromes can appear involving other organs such as cardiovascular and musculoskeletal apparatus due to the deregulation of hormones and cytokines having pleiotropic effects, such as lipocalin 2.[33−35]

It is known that contrary to saturated fats, unsaturated long-chain fatty acids exert anti-inflammatory, antiobesity, and insulin-sensitizing effects by binding to G-protein-coupled receptor 120/free fatty acid receptor 4 (GPR120/FFAR4). For this reason, natural (i.e., docosahexaenoic acid and linoleic

https://doi.org/10.1021/acsomega.4c03507
ACS Omega XXXX, XXX, XXX−XXX

acid) and synthetic (i.e., GSK137647A, TUG-891, PBI-4547, and AH-7614) agonists of GPR-120 are currently emerging as interesting new potential agents to treat metabolic and inflammatory diseases, including obesity, type 2 diabetes, and NAFLD.[36] Despite the interest, nowadays, no GPR120 synthetic agonist is registered in clinical trials (clinicaltrials.gov) due to some limitations such as a short half-life, low oral bioavailability, or high interindividual variability, while natural agonists require massive doses to exert therapeutical effect. In this context, in this study, we tested the effect of a new synthetic agonist of GPR-120 (GprA) in a mouse model of NAFL/NASH induced by WSD administration. This diet also known as the Gubra-Amylin NASH diet has been formulated since saturated fats from palm oil can raise low-density lipoproteins (LDL) cholesterol, causing a fat accumulation in the liver cells; fructose bypasses the rate-limiting steps of glycolysis, leading to increased de novo lipogenesis and uric acid production, which can contribute to inflammation and oxidative stress; finally, high levels of cholesterol can worsen liver inflammation and fibrosis. These dietary factors together contribute to metabolic syndrome in mice, displaying obesity and glucose tolerance issues similar to human NASH.[37] Furthermore, the mouse model has some advantages, primarily the absence of other metabolic complications associated with weight gain, thus eliminating many confounding agents for the evaluation of drug efficacy.

Compared to other synthetic agonists, GprA presents similar or higher in vitro potency as well as receptor selectivity. Other promising ligands are not fully selective toward GPR120, such as PBI-4547, which showed antagonist activity at G-protein-coupled receptor 84 (GPR84), and its beneficial effects resulted abrogated in GPR84-knock out mice.[38] We showed that after 3 weeks of GprA (90 mg/kg), signs of steatosis in the liver parenchyma are reduced both in NAFL and in NASH groups compared to controls, starting with a decrease of perilipin (*per2*) gene expression at 26w and culminating with a reduction of fat content at 30 weeks. Unexpectedly, no striking differences resulted in the inflammatory profile both in the inflammatory score and in gene expression (*il-6* and *il1-β*). A possible explanation is that in our experimental model, the inflammation process is not fully activated yet. Accordingly, the phenotypic data published on the webpage of the mice supplier company showed no significant differences in inflammation scores from 20 to 35 weeks of a diet (https://www.taconic.com/mouse-model/diet-induced-nash-b6).

To better understand the GprA effect on NASH progression, we evaluated the pro-fibrotic molecular profile; Western blot analysis confirmed the decrease in the expression of the *ccn2*, the downstream effector of the cascade of TGF-*β*, and supported the reduction of fibrosis highlighted by Sirius red staining. Accordingly, immunohistochemistry on liver sections confirmed the Col1a1 and Col3a1 decrease in GprA90-treated mice compared to that in the control. This picture is coherently completed by a reduction of *α*-SMA positive hepatic stellate cells (HSCs) in the GprA group compared to that in the control, confirming a decrease in fibrogenesis. In this context, the beneficial effect exerted by GprA on two of the main features of NAFLD, steatosis and fibrosis, is undoubtedly an important step forward in the fight against NAFLD.

We are conscious that it is important to deepen the mechanism of action of GprA. Moreover, we lack a standard diet-fed control group. However, we believe that while these experimental limitations exist, they do not have scientific implications that would prevent the strength and the impact of the drug's effect in the context of fatty liver. Moreover, at the current stage, the present study is a "proof-of-concept" oriented research aimed at investigating the efficacy of the new GprA in the NAFLD background on a small-scale experimental ground. Based on the promising results presented in this paper, it will be interesting to scale up into a wider study to test the safety in a control group and its efficacy on mouse models in which inflammation and fibrosis are more evident, such as the bile duct ligation surgical model or genetically modified mice (Ob/ob mice), as well as models resembling more precisely the metabolic complexity of human NAFLD. Altogether these results prompt us to believe that GprA could be a promising candidate in the development of new therapy in the treatment of these still unresolved and widespread disorders.

AUTHOR INFORMATION

Corresponding Author

Alfredo Cappariello − *Department of Life, Health and Experimental Sciences, University of L'Aquila, 67100 L'Aquila, Italy*; orcid.org/0000-0002-1711-3373; Email: alfredo.cappariello@univaq.it

Authors

Simona Pompili − *Department of Biotechnological and Applied Clinical Sciences, University of L'Aquila, 67100 L'Aquila, Italy*

Antonella Vetuschi − *Department of Biotechnological and Applied Clinical Sciences, University of L'Aquila, 67100 L'Aquila, Italy*

Roberta Sferra − *Department of Biotechnological and Applied Clinical Sciences, University of L'Aquila, 67100 L'Aquila, Italy*

Complete contact information is available at: https://pubs.acs.org/10.1021/acsomega.4c03507

Author Contributions

S.P., A.C., A.V., and R.S. provided equal contribution. A.C. and S.P. have made contributions to the conception and design of the work, in vivo treatment, necroscopy, explant of organs and their photographic documentation, histological evaluation and quantification, acquisition, analysis, interpretation of the data, and drawing of table of contents graphic. A.V. and R.S. have contributed to the analysis and interpretation of the data and revision of the manuscript. All authors read and approved the final manuscript.

Author Contributions

†Equal contribution as first authors.

Author Contributions

‡Equal contribution as last authors.

Funding

This study was funded by intramural DISCAB GRANT 2023 (code 07_DG_2023_20), Department of Biotechnological and Applied Clinical Sciences, University of L'Aquila.

Notes

The authors declare no competing financial interest.

Procedures involving animals and their care were approved by the Ministry of Health at the University of L'Aquila (618/2021-PR reply to CE5C5.37).

LIST OF ABBREVIATIONS

BSA, bovine serum albumin; CO_2, carbon dioxide; EMT, epithelial to mesenchymal transition; FFARs, free fatty acid receptors; FFAs, free fatty acids; FFAR4, free fatty acid receptor

https://doi.org/10.1021/acsomega.4c03507
ACS Omega XXXX, XXX, XXX−XXX

4; GLP1R, glucagon-like peptide 1 receptor; GPCRs, G-protein-coupled receptors; H&E, hematoxylin and eosin; HCC, hepatocarcinoma; HPCs, hepatic progenitor cells; HRP, horseradish peroxidase; HSCs, hepatic stellate cells; IF, immunofluorescence; IR, insulin resistance; NAFL, non-alcoholic fatty liver; NAFLD, nonalcoholic fatty liver disease; NASH, nonalcoholic steatohepatitis; P2 × 3, P2X purinoceptor 3; PBS, phosphate buffer saline; RIPA, radioImmunoPrecipitation; TG, triglycerides; TGR5, takeda G-protein-coupled receptor 5; TRPA1, transient receptor potential cation channel, subfamily A, member 1; TRPV4, transient receptor potential vanilloid 4; VLDL, very low-density lipoproteins; WSD, Western-style diet; α-SMA, smooth muscle alpha-actin; ω3-FAs, omega-3 fatty acids

REFERENCES

(1) Mallah, M. A.; Soomro, T.; Noreen, S.; Ali, M.; Kafle, A.; Khatoon, N.; et al. Association of obesity and cardiovascular disease and progress in pharmacotherapy: what is next for obesity? *Int. J. Rehabil Res.* **2023**, *46* (1), 14−25.

(2) Mantovani, A.; Petracca, G.; Beatrice, G.; Tilg, H.; Byrne, C. D.; Targher, G. Non-alcoholic fatty liver disease and risk of incident diabetes mellitus: an updated meta-analysis of 501 022 adult individuals. *Gut.* **2021**, *70* (5), 962−969.

(3) Artymiak, P.; Żegleń, M.; Kowal, M.; Woronkowicz, A.; Kryst, Ł Changes in the prevalence of underweight, overweight, obesity and excessive adiposity among adolescents from Kraków (Poland) in the years 1983−2020. *Am. J. Hum. Biol.* **2023**, *35*, No. e23866, DOI: 10.1002/ajhb.23866.

(4) Blad, C. C.; Tang, C.; Offermanns, S. G protein-coupled receptors for energy metabolites as new therapeutic targets. *Nat. Rev. Drug Discovery* **2012**, *11* (8), 603−619.

(5) Soret, P. A.; Magusto, J.; Housset, C.; Gautheron, J. In Vitro and In Vivo Models of Non-Alcoholic Fatty Liver Disease: A Critical Appraisal. *J. Clin Med.* **2021**, *10* (1), 36.

(6) Peng, C.; Stewart, A. G.; Woodman, O. L.; Ritchie, R. H.; Qin, C. X. Non-Alcoholic Steatohepatitis: A Review of Its Mechanism Models and Medical Treatments. *Front. Pharmacol.* **2020**, *11*, No. 603926.

(7) Hara, T.; Hirasawa, A.; Ichimura, A.; Kimura, I.; Tsujimoto, G. Free fatty acid receptors FFAR1 and GPR120 as novel therapeutic targets for metabolic disorders. *J. Pharm. Sci.* **2011**, *100* (9), 3594−3601.

(8) Rosenbaum, D. M.; Rasmussen, S. G. F.; Kobilka, B. K. The structure and function of G-protein-coupled receptors. *Nature.* **2009**, *459* (7245), 356−363.

(9) Song, T.; Yang, Y.; Zhou, Y.; Wei, H.; Peng, J. GPR120: a critical role in adipogenesis, inflammation, and energy metabolism in adipose tissue. *Cell. Mol. Life Sci.* **2017**, *74* (15), 2723−2733.

(10) Ichimura, A.; Hirasawa, A.; Poulain-Godefroy, O.; Bonnefond, A.; Hara, T.; Yengo, L.; et al. Dysfunction of lipid sensor GPR120 leads to obesity in both mouse and human. *Nature.* **2012**, *483* (7389), 350−354.

(11) Eslam, M.; Newsome, P. N.; Sarin, S. K.; Anstee, Q. M.; Targher, G.; Romero-Gomez, M.; et al. A new definition for metabolic dysfunction-associated fatty liver disease: An international expert consensus statement. *J. Hepatol.* **2020**, *73* (1), 202−209.

(12) Tessitore, A.; Mastroiaco, V.; Vetuschi, A.; Sferra, R.; Pompili, S.; Cicciarelli, G.; et al. Development of hepatocellular cancer induced by long term low fat-high carbohydrate diet in a NAFLD/NASH mouse model. *Oncotarget.* **2017**, *8* (32), 53482−53494.

(13) Pompili, S.; Vetuschi, A.; Gaudio, E.; Tessitore, A.; Capelli, R.; Alesse, E.; et al. Long-term abuse of a high-carbohydrate diet is as harmful as a high-fat diet for development and progression of liver injury in a mouse model of NAFLD/NASH. *Nutrition* **2020**, *75-76*, No. 110782.

(14) Sferra, R.; Pompili, S.; Cappariello, A.; Gaudio, E.; Latella, G.; Vetuschi, A. Prolonged Chronic Consumption of a High Fat with Sucrose Diet Alters the Morphology of the Small Intestine. *Int. J. Mol. Sci.* **2021**, *22* (14), 7280−7294.

(15) Vetuschi, A.; Cappariello, A.; Onori, P.; Gaudio, E.; Latella, G.; Pompili, S.; et al. Ferroptosis resistance cooperates with cellular senescence in the overt stage of nonalcoholic fatty liver disease/nonalcoholic steatohepatitis. *Eur. J. Histochem.* **2022**, *66* (3), 3391 DOI: 10.4081/ejh.2022.3391.

(16) Di Minno, M. N. D.; Russolillo, A.; Lupoli, R.; Ambrosino, P.; Di Minno, A.; Tarantino, G. Omega-3 fatty acids for the treatment of non-alcoholic fatty liver disease. *World J. Gastroenterol.* **2012**, *18* (41), 5839−5847.

(17) Jump, D. B.; Lytle, K. A.; Depner, C. M.; Tripathy, S. Omega-3 polyunsaturated fatty acids as a treatment strategy for nonalcoholic fatty liver disease. *Pharmacol Ther.* **2018**, *181*, 108−125.

(18) Li, Y.; Xu, H.; Wu, W.; Ye, J.; Fang, D.; Shi, D.; et al. Clinical application of angiotensin receptor blockers in patients with non-alcoholic fatty liver disease: a systematic review and meta-analysis. *Oncotarget.* **2018**, *9* (35), 24155−24167.

(19) Woods, C. P.; Hazlehurst, J. M.; Tomlinson, J. W. Glucocorticoids and non-alcoholic fatty liver disease. *J. Steroid Biochem. Mol. Biol.* **2015**, *154*, 94−103.

(20) Ndakotsu, A.; Vivekanandan, G. The Role of Thiazolidinediones in the Amelioration of Nonalcoholic Fatty Liver Disease: A Systematic Review. *Cureus* **2022**, *14* (5), No. e25380, DOI: 10.7759/cureus.25380.

(21) Boutari, C.; Pappas, P. D.; Anastasilakis, D.; Mantzoros, C. S. Statins' efficacy in non-alcoholic fatty liver disease: A systematic review and meta-analysis. *Clin Nutr.* **2022**, *41* (10), 2195−2206.

(22) Cioboată, R.; Găman, A.; Trașcă, D.; Ungureanu, A.; Docea, A. O.; Tomescu, P.; et al. Pharmacological management of non-alcoholic fatty liver disease: Atorvastatin versus pentoxifylline. *Exp Ther Med.* **2017**, *13* (5), 2375−2381.

(23) Kleiner, D. E.; Brunt, E. M.; Van Natta, M.; Behling, C.; Contos, M. J.; Cummings, O. W.; et al. Design and validation of a histological scoring system for nonalcoholic fatty liver disease. *Hepatology.* **2005**, *41* (6), 1313−1321.

(24) Bedossa, P.; Poitou, C.; Veyrie, N.; Bouillot, J. L. L.; Basdevant, A.; Paradis, V.; et al. Histopathological algorithm and scoring system for evaluation of liver lesions in morbidly obese patients. *Hepatology.* **2012**, *56* (5), 1751−1759.

(25) Heyens, L. J. M.; Busschots, D.; Koek, G. H.; Robaeys, G.; Francque, S. Liver Fibrosis in Non-alcoholic Fatty Liver Disease: From Liver Biopsy to Non-invasive Biomarkers in Diagnosis and Treatment. *Front. Med. (Lausanne)* **2021**, *8*, No. 615978.

(26) Lefere, S.; Tacke, F. Macrophages in obesity and non-alcoholic fatty liver disease: Crosstalk with metabolism. *JHEP Rep.* **2019**, *1* (1), 30−43.

(27) Gastaldelli, A.; Cusi, K.; Pettiti, M.; Hardies, J.; Miyazaki, Y.; Berria, R.; et al. Relationship between hepatic/visceral fat and hepatic insulin resistance in nondiabetic and type 2 diabetic subjects. *Gastroenterology.* **2007**, *133* (2), 496−506.

(28) Brunt, E. M.; Wong, V. W. S.; Nobili, V.; Day, C. P.; Sookoian, S.; Maher, J. J.; et al. Nonalcoholic fatty liver disease. *Nat. Rev. Dis. Primers* **2015**, *1*, 15080 DOI: 10.1038/nrdp.2015.80.

(29) Musso, G.; Cassader, M.; Paschetta, E.; Gambino, R. Bioactive Lipid Species and Metabolic Pathways in Progression and Resolution of Nonalcoholic Steatohepatitis. *Gastroenterology* **2018**, *155* (2), 282−302.e8.

(30) Tomita, K.; Tamiya, G.; Ando, S.; Ohsumi, K.; Chiyo, T.; Mizutani, A.; et al. Tumour necrosis factor alpha signalling through activation of Kupffer cells plays an essential role in liver fibrosis of non-alcoholic steatohepatitis in mice. *Gut.* **2006**, *55* (3), 415−424.

(31) Herck, M. A. V.; Weyler, J.; Kwanten, W. J.; Dirinck, E. L.; Winter, B. Y. D.; Francque, S. M.; et al. The Differential Roles of T Cells in Non-alcoholic Fatty Liver Disease and Obesity. *Front. Immunol.* **2019**, *10*, 82 DOI: 10.3389/fimmu.2019.00082.

(32) Roehlen, N.; Crouchet, E.; Baumert, T. F. Liver Fibrosis: Mechanistic Concepts and Therapeutic Perspectives. *Cells* **2020**, *9* (4), 875 DOI: 10.3390/cells9040875.

https://doi.org/10.1021/acsomega.4c03507
ACS Omega XXXX, XXX, XXX−XXX

(33) Kim, K. E.; Lee, J.; Shin, H. J.; Jeong, E. A.; Jang, H. M.; Ahn, Y. J.; et al. Lipocalin-2 activates hepatic stellate cells and promotes nonalcoholic steatohepatitis in high-fat diet-fed Ob/Ob mice. *Hepatology* **2023**, *77* (3), 888−901. https://pubmed.ncbi.nlm.nih.gov/35560370/

(34) Rucci, N.; Capulli, M.; Piperni, S. G.; Cappariello, A.; Lau, P.; Frings-Meuthen, P.; et al. Lipocalin 2: A new mechanoresponding gene regulating bone homeostasis. *J. Bone Miner. Res.* **2015**, *30* (2), 357−368, DOI: 10.1002/jbmr.2341.

(35) Ponzetti, M.; Aielli, F.; Ucci, A.; Cappariello, A.; Lombardi, G.; Teti, A.; et al. Lipocalin 2 increases after high-intensity exercise in humans and influences muscle gene expression and differentiation in mice. *J. Cell Physiol* **2022**, *237* (1), 551.

(36) Milligan, G.; Alvarez-Curto, E.; Hudson, B. D.; Prihandoko, R.; Tobin, A. B. FFA4/GPR120: Pharmacology and Therapeutic Opportunities. *Trends Pharmacol. Sci.* **2017**, *38* (9), 809−821.

(37) Hansen, H. H.; Ægidius, H. M.; Oró, D.; Evers, S. S.; Heebøll, S.; Eriksen, P. L.; et al. Human translatability of the GAN diet-induced obese mouse model of non-alcoholic steatohepatitis. *BMC Gastroenterol.* **2020**, *20* (1), 210 DOI: 10.1186/s12876-020-01356-2. https://bmcgastroenterol.biomedcentral.com/articles/10.1186/s12876-020-01356-2

(38) Simard, J. C.; Thibodeau, J. F.; Leduc, M.; Tremblay, M.; Laverdure, A.; Sarra-Bournet, F.; et al. Fatty acid mimetic PBI-4547 restores metabolic homeostasis via GPR84 in mice with non-alcoholic fatty liver disease. *Sci. Rep.* **2020**, *10* (1), 12778.

https://doi.org/10.1021/acsomega.4c03507
ACS Omega XXXX, XXX, XXX−XXX